Earthquakes and Structures, *Vol. 13, No. 6 (2017) 589-598*
DOI: https://doi.org/10.12989/eas.2017.13.6.589

Dynamic response of concrete beams reinforced by Fe_2O_3 nanoparticles subjected to magnetic field and earthquake load

Hossein Mohammadian, Reza Kolahchi* and Mahmood Rabani Bidgoli

Department of Civil Engineering, Jasb Branch, Islamic Azad University, Jasb, Iran

(Received September 13, 2017, Revised January 11, 2018, Accepted January 16, 2018)

Abstract. In this paper, dynamic response of the horizontal concrete beam subjected to seismic ground excitation is investigated. The structure is reinforced by Fe_2O_3 nanoparticles which have the magnetic properties. The hyperbolic shear deformation beam theory (HSDBT) is used for mathematical modeling of the structure. Based on the Mori-Tanaka model, the effective material properties of concrete beam is calculated considering the agglomeration of Fe_2O_3 nanoparticles. Applying energy method and Hamilton's principle, the motion equations are derived. Harmonic differential quadrature method (HDQM) along with Newmark method is utilized for numerical solution of the motion equations. The effects of different parameters such as volume fraction and agglomeration of Fe_2O_3 nanoparticles, magnetic field, boundary conditions and geometrical parameters of concrete beam are studied on the dynamic response of the structure. In order to validation of this work, an exact solution is used for comparing the numerical and analytical results. The results indicated that applying magnetic field decreases the of the structure up to 54 percent. In addition, increase too much the magnetic field (Hx>5e8 A/m) does not considerable effect on the reduction of the maximum dynamic displacement.

Keywords: dynamic response; Fe_2O_3 nanoparticles; seismic ground excitation; HDQM; magnetic field

1. Introduction

Nano-engineered cement based materials is actual tends which could play an important role for efficient use of this binder, recently many oxide nanoparticles like nano-SiO_2, nano-TiO_2, nano-Fe_2O_3, nano-Al_2O_3, nano-$CaCO_3$, nano-ZnO, nano-cement particles of C_2S (alita) and C_3S (belite), nano-clays and Carbon Nanotubes have been tested, those improve the cement based materials performance. Although, nano-particles have a unitary coast 100 to 1000 times bigger than the Portland cement or others conventional raw-materials employed for cement based materials production, an important economic aspect for material design.

Liang and Parra-Montesinos (2004) studied seismic behavior of four reinforced concrete column-steel beam under various ground motions using experimental tests. Cheng and Chen (2004), Changwang *et al*. (2010) studied seismic behavior of steel reinforced concrete column-steel truss beam. They developed a design formula for shear strength of the structure subjected to seismic activities using experimental tests. The effect of cumulative damage on the seismic behavior of steel tube-reinforced concrete (ST-RC) columns through experimental testing was investigated by Ji *et al*. (2014). Six large-scale ST-RC column specimens were subjected to high axial forces and cyclic lateral loading. The effect of plastic hinge relocation on the potential damage of a reinforced concrete frame subjected to different seismic levels was studied by Cao and Ronagh (2014) based on current seismic designs. The optimal seismic retrofit method that uses FRP jackets for shear-critical RC frames was presented by Choi *et al*. (2014). This optimal method uses non-dominated sorting genetic algorithm-II (NSGA-II) to optimize the two conflicting objective functions of the retrofit cost as well as the seismic performance, simultaneously. They examined various parameters like, failure mode, hysteresis curves, ductility and reduction of stiffness. Liu *et al*. (2016) focused on the study of seismic behavior of steel reinforced concrete special-shaped column-beam joints. Six specimens, which are designed according to the principle of strong-member and weak-joint core, are tested under low cyclic reversed load.

In none of the above articles, the nanocomposite structure is considered. Wuite and Adali (2005) performed stress analysis of carbon nanotubes (CNTs) reinforced beams. They concluded that using CNTs as reinforcing phase can increase the stiffness and the stability of the system. Also, Matsunaga (2007) examined stability of the composite cylindrical shell using third-order shear deformation theory (TSDT). Formica *et al*. (2010) analyzed vibration behavior of CNTs reinforced composites. They employed an equivalent continuum model based onEshelby-Mori-Tanaka model to obtain the material properties of the composite. Liew *et al*. (2014) studied postbuckling of nanocomposite cylindrical panels. They used the extended rule of mixture to estimate the effective material properties of the nanocomposite structure. They also applied a meshless approach to examine the postbuckling response of the nanocomposite cylindrical panel. In another similar work, Lei *et al*. (2014) studied dynamic stability of a CNTs reinforced functionally graded (FG) cylindrical panel. They

*Corresponding author, Ph.D.
E-mail: r.kolahchi@gmail.com

Copyright © 2017 Techno-Press, Ltd.

ISSN: 2092-7614 (Print), 2092-7622 (Online)

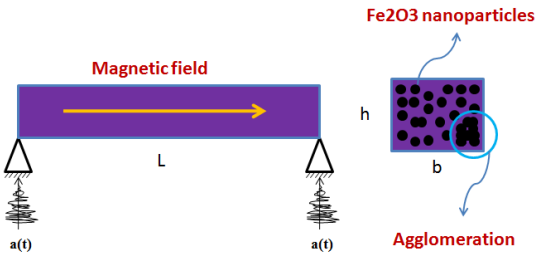

Fig. 1 A schematic figure of concrete beam reinforced by agglomerated Fe_2O_3 nanoparticles under magnetic field

used Eshelby-Mori-Tanaka model to estimate effective material properties of the resulting nanocomposite structure and also employed Ritz method to distinguish the instability regions of the structure. Static stress analysis of CNTs reinforced cylindrical shells is presented by Ghorbanpour Arani *et al*. (2015). In this work, the cylindrical shell was subjected to non-axisymmetric thermal-mechanical loads and uniform electro-magnetic fields. Eventually, the stress distribution in the structure is determined analytically by Fourier series. Buckling analysis of CNTs reinforced microplates is carried out by Kolahchi *et al*. (2013). They derived the governing equations of the structure based on Mindlin plate theory and using Hamilton's principle. They obtained buckling load of the structure by applying differential quadrature method (DQM). Dynamic response of FG circular cylindrical shells is examined by Davar *et al*. (2013). They developed the mathematical formulation of the structure according to first order shear deformation theory (FSDT) and Love's first approximation theory. Also, Kolahchi *et al*. (2016) investigated dynamic stability of FG-CNTs reinforced plates. The material properties of the plate are assumed to be a function of temperature and the structure is considered resting on orthotropic elastomeric medium. Jafarian Arani and Kolahchi (2016) presented a mathematical model for buckling analysis of a CNTs reinforced concrete column. They simulated the problem based on Euler Bernoulli and Timoshenko beam theories.Nonlinear vibration of laminated cylindrical shells is analyzed by Shen and Yang (2014). They examined the influences of temperature variation, shell geometric parameter and applied voltage on the linear and nonlinear vibration of the structure. Alibeigloo (2016) employed theory of piezo-elasticity to study bending behavior of FG-CNTs reinforced composite cylindrical panels. They used an analytical method to study the effect of CNT volume fraction, temperature variation and applied voltage on the bending behavior of the system. Feng *et al*. (2017) studied the nonlinear bending behavior of a novel class of multi-layer polymer nanocomposite beams reinforced with graphene platelets (GPLs) that are non-uniformly distributed along the thickness direction. Zamani *et al*. (2017) studied seismic response of pipes is examined by applying nanotechnology and piezoelectric materials. For this purpose, a pipe is considered which is reinforced by carbon nanotubes (CNTs) and covered with a piezoelectric layer. Sharif Zarei *et al*. (2017) studied seismic response of thefluid-conveying concrete pipes reinforced with SiO_2 nanoparticles andfiber reinforced polymer (FRP) layer.

For the first time, dynamic response of Fe_2O_3 nanoparticles-reinforced concrete beams subjected to seismic excitation and magnetic field is studied in the present research. So, the results of this research are of great importance in Civil Engineering. The concrete beam is modeled by applying HSDBT and the effective material properties of the concrete beam are obtained based on Mori-Tanaka model considering agglomeration of Fe_2O_3 nanoparticles. The dynamic displacement of structure is calculated by HDQM in conjunction with Newmark method. The effects of different parameters such as volume fraction and agglomeration of Fe_2O_3 nanoparticles, magnetic field, boundary conditions and geometrical parameters of concrete beam are studied on the dynamic response of the structure.

2. Formulation

2.1 Strain relations

As shown in Fig. 1, a concrete beam is reinforced by agglomerated Fe_2O_3 nanoparticles subjected to the earthquake load and magnetic field. The geometrical parameters of beam are length of L and thickness of h.

By applying HSDBT, the displacements fields are defined as below (Simsek and Reddy 2013)

$$\begin{aligned} u_1(x,z) &= U(x) - z\frac{\partial W(x)}{\partial x} + \Phi(z)\left(\frac{\partial W(x)}{\partial x} - \phi(x)\right), \\ u_2(x,z) &= 0, \\ u_3(x,z) &= W(x), \end{aligned} \tag{1}$$

where U, V and W are the respective translation displacements of a point at the mid-plane of the beam in the longitudinal x, transverse y and thickness z directions. Also, ϕ denotes the rotation of the cross section area and $\Phi(z)$ is the shape function of the beam which is considered as follows

$$\Phi(z) = h\sinh\left(\frac{z}{h}\right) - z\cosh\left(\frac{1}{2}\right), \tag{2}$$

However, the strain-displacement relations of the structure are given as below

$$\varepsilon_{xx} = \left(\frac{\partial U}{\partial x}\right) + \left(\frac{1}{2}\left(\frac{\partial W}{\partial x}\right)^2\right) - z\left(\frac{\partial^2 W}{\partial x^2}\right) + \Phi(z)\left(\frac{\partial^2 W}{\partial x^2} - \frac{\partial \phi}{\partial x}\right), \tag{3}$$

$$\gamma_{xz} = \frac{\partial \Phi(z)}{\partial z}\left(\frac{\partial W}{\partial x} - \phi\right). \tag{4}$$

2.2 Stress relations

The constitutive equations of the orthotropic beam are considered as below

$$\sigma_{xx} = C_{11}\varepsilon_{xx}, \tag{5}$$

$$\tau_{xz} = C_{44}\gamma_{xz}, \tag{6}$$

where C_{11} and C_{44} are the elastic constants of the concrete beam. To obtain the effective material properties of the concrete beam and to consider the agglomeration effect, Mori-Tanak model (Mori andTanak 1973) is employed which the effective Young's modulus E and Poisson's ratio v of the composite material are given by

$$E = \frac{9KG}{3K+G} \quad , \tag{32}$$

$$\upsilon = \frac{3K-2G}{6K+2G}. \tag{33}$$

where the effective bulk modulus K and shear modulus G may be written as below (Shu and Xue 1997)

$$K = K_{out}\left[1+\frac{\xi\left(\frac{K_{in}}{K_{out}}-1\right)}{1+\alpha(1-\xi)\left(\frac{K_{in}}{K_{out}}-1\right)}\right] \quad , \tag{17}$$

$$G = G_{out}\left[1+\frac{\xi\left(\frac{G_{in}}{G_{out}}-1\right)}{1+\beta(1-\xi)\left(\frac{G_{in}}{G_{out}}-1\right)}\right], \tag{18}$$

The agglomeration effect can be considered based on the micro-mechanical model by introducing the two following parameters

$$\xi = \frac{V_{inclusion}}{V}, \tag{12}$$

$$\zeta = \frac{V_r^{inclusion}}{V_r}. \tag{13}$$

where V_r and $V_r^{inclusion}$ are the total volume of nanoparticles and volume of the nanoparticles inside the inclusion, respectively. in addition, K_{in} and K_{out} are the effective bulk modulus of the inclusion and the matrix outside the inclusion, respectively. Also, G_{in} and G_{out} are the effective shear modulus of the inclusion and the matrix outside the inclusion, respectively and are given as follows

$$K_{in} = K_m + \frac{(\delta_r - 3K_m\chi_r)C_r\zeta}{3(\xi - C_r\zeta + C_r\zeta\chi_r)}, \tag{19}$$

$$K_{out} = K_m + \frac{C_r(\delta_r - 3K_m\chi_r)(1-\zeta)}{3\left[1-\xi-C_r(1-\zeta)+C_r\chi_r(1-\zeta)\right]}, \tag{20}$$

$$G_{in} = G_m + \frac{(\eta_r - 3G_m\beta_r)C_r\zeta}{2(\xi - C_r\zeta + C_r\zeta\beta_r)}, \tag{21}$$

$$G_{out} = G_m + \frac{C_r(\eta_r - 3G_m\beta_r)(1-\zeta)}{2\left[1-\xi-C_r(1-\zeta)+C_r\beta_r(1-\zeta)\right]}, \tag{22}$$

where C_r is the volume percent of nanoparticles and χ_r, β_r, δ_r and η_r can be obtained as

$$\chi_r = \frac{3(K_m+G_m)+k_r-l_r}{3(k_r+G_m)}, \tag{23}$$

$$\beta_r = \frac{1}{5}\left\{\begin{array}{l}\frac{4G_m+2k_r+l_r}{3(k_r+G_m)}+\frac{4G_m}{(p_r+G_m)}\\ +\frac{2\left[G_m(3K_m+G_m)+G_m(3K_m+7G_m)\right]}{G_m(3K_m+G_m)+m_r(3K_m+7G_m)}\end{array}\right\}, \tag{24}$$

$$\delta_r = \frac{1}{3}\left[n_r+2l_r+\frac{(2k_r-l_r)(3K_m+2G_m-l_r)}{k_r+G_m}\right], \tag{25}$$

$$\eta_r = \frac{1}{5}\left[\begin{array}{l}\frac{2}{3}(n_r-l_r)+\frac{4G_mp_r}{(p_r+G_m)}+\frac{2(k_r-l_r)(2G_m+l_r)}{3(k_r+G_m)}\\ +\frac{8G_mm_r(3K_m+4G_m)}{3K_m(m_r+G_m)+G_m(7m_r+G_m)}\end{array}\right], \tag{26}$$

in which k_r, l_r, n_r, p_r and m_r are Hill's elastic moduli of the reinforcing phase of the composite material. Furthermore, K_m and G_m are the bulk and shear moduli of the matrix phase which are defined as below

$$K_m = \frac{E_m}{3(1-2\upsilon_m)} \quad , \tag{27}$$

$$G_m = \frac{E_m}{2(1+\upsilon_m)}. \tag{28}$$

where E_m and v_m are considered as Young's modulus and Poisson's ratio of the concrete beam, respectively. Moreover, α and β in Eqs. (17) and (18) are given as follows

$$\alpha = \frac{(1+\upsilon_{out})}{3(1-\upsilon_{out})} \quad , \tag{29}$$

$$\alpha = \frac{(1+\upsilon_{out})}{3(1-\upsilon_{out})} \quad , \tag{30}$$

$$\upsilon_{out} = \frac{3K_{out}-2G_{out}}{6K_{out}+2G_{out}}. \tag{31}$$

2.3 Energy method

The potential strain energy stored in the structure is given as follows

$$U = \int_V \left(\sigma_{xx}\varepsilon_{xx} + \tau_{xz}\gamma_{xz}\right)dA\,dx, \tag{34}$$

Substituting Eqs. (3) and (4) into Eq. (34) we have

$$\begin{aligned}U = \frac{1}{2}\int_0^L\Bigg[\int\Bigg[N_x\left(\left(\frac{\partial U}{\partial x}\right)+\left(\frac{1}{2}\left(\frac{\partial W}{\partial x}\right)^2\right)\right)-M_x\left(\frac{\partial^2 W}{\partial x^2}\right)\\ +F_x\left(\frac{\partial^2 W}{\partial x^2}-\frac{\partial\phi}{\partial x}\right)+Q_x\left(\left(\frac{\partial W}{\partial x}-\phi\right)\right)\Bigg]\Bigg]dx,\end{aligned} \tag{35}$$

where

$$N_x = \int_A \sigma_{xx} dA, \tag{36}$$

$$M_x = \int_A \sigma_{xx} z dA, \tag{37}$$

$$F_x = \int_A \sigma_{xx} \Phi(z) dA, \tag{38}$$

$$Q_x = \int_A \tau_{xz} \frac{\partial \Phi(z)}{\partial z} dA, \tag{39}$$

By substituting Eqs. (5)-(8) into Eqs. (36)-(39), the stress resultants of the beam take the following form

$$N_x = A_{11}\left(\frac{\partial U}{\partial x} + \frac{1}{2}\left(\frac{\partial W}{\partial x}\right)^2\right) - B_{11}\left(\frac{\partial^2 W}{\partial x^2}\right) + E_{11}\left(\frac{\partial^2 W}{\partial x^2} - \frac{\partial \varphi}{\partial x}\right), \tag{41}$$

$$M_x = B_{11}\left(\frac{\partial U}{\partial x} + \frac{1}{2}\left(\frac{\partial W}{\partial x}\right)^2\right) - D_{11}\left(\frac{\partial^2 W}{\partial x^2}\right) + F_{11}\left(\frac{\partial^2 W}{\partial x^2} - \frac{\partial \varphi}{\partial x}\right), \tag{42}$$

$$F_x = E_{11}\left(\frac{\partial U}{\partial x} + \frac{1}{2}\left(\frac{\partial W}{\partial x}\right)^2\right) - F_{11}\left(\frac{\partial^2 W}{\partial x^2}\right) + H_{11}\left(\frac{\partial^2 W}{\partial x^2} - \frac{\partial \varphi}{\partial x}\right), \tag{43}$$

$$Q_x = L_{44}\left(\frac{\partial W}{\partial x} - \phi\right), \tag{44}$$

in which

$$A_{11} = \int_A C_{11} dA, \tag{45}$$

$$B_{11} = \int_{A_c} C_{11} z dA_c + \int_{A_f} Q_{11} z dA_f, \tag{46}$$

$$B_{11} = \int_A C_{11} z dA, \tag{47}$$

$$D_{11} = \int_A C_{11} z^2 dA, \tag{48}$$

$$E_{11} = \int_A C_{11} \Phi(z) dA, \tag{49}$$

$$F_{11} = \int_A C_{11} z \Phi(z) dA, \tag{50}$$

$$H_{11} = \int_A C_{11} \Phi(z)^2 dA, \tag{51}$$

The kinetic energy of the structure are defined as below

$$K = \frac{\rho}{2}\int \left(\dot{u}_1^2 + \dot{u}_2^2 + \dot{u}_3^2\right) dV \tag{52}$$

By substituting Eq. (1) into Eq. (52) we have

$$K = 0.5\int \left[I_0\left(\left(\frac{\partial U}{\partial t}\right)^2 + \left(\frac{\partial W}{\partial t}\right)^2\right) - 2I_1\left(\frac{\partial U}{\partial t}\frac{\partial^2 W}{\partial x \partial t}\right) + I_2\left(\frac{\partial^2 W}{\partial x \partial t}\right)^2 + I_3\frac{\partial U}{\partial t}\left(\frac{\partial^2 W}{\partial x \partial t} - \frac{\partial \varphi}{\partial t}\right) - I_4\frac{\partial^2 W}{\partial x \partial t}\left(\frac{\partial^2 W}{\partial x \partial t} - \frac{\partial \varphi}{\partial t}\right) + I_5\left(\frac{\partial^2 W}{\partial x \partial t} - \frac{\partial \varphi}{\partial t}\right)^2\right] dx. \tag{53}$$

where

$$\begin{Bmatrix} I_0 \\ I_1 \\ I_2 \\ I_3 \\ I_4 \\ I_5 \end{Bmatrix} = \int_A \begin{bmatrix} \rho \\ \rho z \\ \rho z^2 \\ \rho \Phi(z) \\ \rho z \Phi(z) \\ \rho \Phi(z)^2 \end{bmatrix} dA, \tag{54}$$

The external work due the earthquake and magnetic field can be calculated as follows (Kolahchi *et al*. 2016)

$$W = \int (ma(t) + \mu H_x^2 h \frac{\partial^2 w}{\partial x^2}) W dx, \tag{56}$$

where m and $a(t)$ are the mass and acceleration of the earth, respectively; μ and H_x are magnetic permeability and magnetic field, respectively. To extract the governing equations of motion, Hamilton's principle is expressed as follows

$$\int_0^t (\delta U - \delta K - \delta W) dt = 0, \tag{57}$$

where δ denotes the variational operator. Substituting Eqs. (58)-(60) into Eq. (57), the motion equations of the structure are obtained as follows

δU :

$$\frac{\partial N_x}{\partial x} = I_0 \frac{\partial^2 U}{\partial t^2} + (I_3 - I_1)\frac{\partial^3 W}{\partial x \partial t^2} - I_3 \frac{\partial^2 \varphi}{\partial t^2}, \tag{61}$$

$$\delta W : \frac{\partial^2 M_x}{\partial x^2} - \frac{\partial}{\partial x}\left(N_x^M \frac{\partial W}{\partial x}\right) - \frac{\partial^2 F_x}{\partial x^2} + \frac{\partial Q_x}{\partial x} + ma(t) + \mu H_x^2 h \frac{\partial^2 w}{\partial x^2} = I_0 \frac{\partial^2 W}{\partial t^2} + (I_1 - I_3)\frac{\partial^3 U}{\partial x \partial t^2} + (2I_4 - I_2 - I_5)\frac{\partial^4 W}{\partial x^2 \partial t^2} + (I_5 - I_4)\frac{\partial^3 \varphi}{\partial x \partial t^2}, \tag{62}$$

$\delta \varphi$:

$$Q_x - \frac{\partial F_x}{\partial x} = I_5 \frac{\partial^2 \varphi}{\partial t^2} - I_3 \frac{\partial^2 U}{\partial t^2} + (I_4 - I_5)\frac{\partial^3 W}{\partial x \partial t^2}, \tag{63}$$

By substituting Eqs. (41)-(44) into Eqs. (61)-(63), the governing equations of the system are expressed as follows

$$\delta U : A_{11}\left(\frac{\partial^2 U}{\partial x^2} + \frac{\partial W}{\partial x}\frac{\partial^2 W}{\partial x^2}\right) - B_{11}\left(\frac{\partial^3 W}{\partial x^3}\right) + E_{11}\left(\frac{\partial^3 W}{\partial x^3} - \frac{\partial^2 \varphi}{\partial x^2}\right) = I_0 \frac{\partial^2 U}{\partial t^2} + (I_3 - I_1)\frac{\partial^3 W}{\partial x \partial t^2} - I_3 \frac{\partial^2 \varphi}{\partial t^2}, \tag{64}$$

$$\begin{aligned}
&\delta W: (B_{11}-E_{11})\left(\frac{\partial^3 U}{\partial x^3}+\left(\frac{\partial^2 W}{\partial x^2}\right)^2+\frac{\partial W}{\partial x}\frac{\partial^3 W}{\partial x^3}\right)\\
&-(D_{11}-F_{11})\left(\frac{\partial^4 W}{\partial x^4}\right)+(F_{11}-H_{11})\left(\frac{\partial^4 W}{\partial x^4}-\frac{\partial^3 \varphi}{\partial x^3}\right)\\
&+L_{44}\left(\frac{\partial^2 W}{\partial x^2}-\frac{\partial \varphi}{\partial x}\right)+F_{Seismic}+\mu \mathrm{H}_x^2\, h\frac{\partial^2 w}{\partial x^2}=I_0\frac{\partial^2 W}{\partial t^2}\\
&+(I_1-I_3)\frac{\partial^3 U}{\partial x\,\partial t^2}+(2I_4-I_2-I_5)\frac{\partial^4 W}{\partial x^2\partial t^2}+(I_5-I_4)\frac{\partial^3 \varphi}{\partial x\,\partial t^2},
\end{aligned} \tag{65}$$

$$\begin{aligned}
&\delta\varphi: Q_x-E_{11}\left(\frac{\partial^2 U}{\partial x^2}+\frac{\partial W}{\partial x}\frac{\partial^2 W}{\partial x^2}\right)+F_{11}\left(\frac{\partial^3 W}{\partial x^3}\right)\\
&-H_{11}\left(\frac{\partial^3 W}{\partial x^3}-\frac{\partial^2 \varphi}{\partial x^2}\right)=I_5\frac{\partial^2 \varphi}{\partial t^2}\\
&-I_3\frac{\partial^2 U}{\partial t^2}+(I_4-I_5)\frac{\partial^3 W}{\partial x\,\partial t^2},
\end{aligned} \tag{66}$$

Also, the boundary conditions of the structure are considered as below

• Clamped-Clamped supported

$$\begin{aligned}
&W=U=\phi=\frac{\partial W}{\partial x}=0, && @\quad x=0\\
&W=U=\phi=\frac{\partial W}{\partial x}=0. && @\quad x=L
\end{aligned} \tag{67}$$

• Clamped-Simply supported

$$\begin{aligned}
&W=U=\phi=\frac{\partial W}{\partial x}=0, && @\quad x=0\\
&W=U=\phi=M_x=0. && @\quad x=L
\end{aligned} \tag{68}$$

• Simply-Simply supported

$$\begin{aligned}
&W=U=\phi=M_x=0, && @\quad x=0\\
&W=U=\phi=M_x=0. && @\quad x=L
\end{aligned} \tag{69}$$

• Clamped-Free

$$\begin{aligned}
&W=U=\phi=\frac{\partial W}{\partial x}=0, && @\quad x=0\\
&F_x=Q_x=N_x=M_x=0. && @\quad x=L
\end{aligned} \tag{70}$$

5. Solution procedure

In this study, HDQM is applied to examine the dynamic behavior of the structure. In this numerical method, the governing differential equations of the structure turn into a set of first order algebraic equations by applying the weighting coefficients. According to HDQ method, a derivative of a function at a given discrete point will be approximated as a weighted linear sum of the function values at all discrete points chosen in the solution domain. The one-dimensional derivative of the function can be expressed as follows (Kolahchi *et al*. 2016)

$$\frac{d^n f(x_i)}{dx^n}=\sum_{j=1}^{N} C_{ij}^{(n)} f(x_j) \qquad n=1,...,N-1. \tag{71}$$

Where $f(x)$ is the mentioned function, N denotes number of grid points, x_i is a sample point of the function domain, f_i is the value of the function at ith sample point and C_{ij}indicates the weighting coefficients. So, choosing the grid points and weighting coefficients is an important factor in the accuracy of the results. The grid points are considered by Chebyshev polynomials as follows

$$X_i=\frac{L}{2}\left[1-\cos\left(\frac{i-1}{N_x-1}\right)\pi\right] \qquad i=1,...,N_x \tag{72}$$

Based on Chebyshev polynomials, the grid points are closer together near the borders and in distant parts of the borders they away from each other. The weighting coefficients may be calculated by the following simple algebraic relations

$$A_{ij}^{(1)}=\begin{cases}\dfrac{(\pi/2)M(x_i)}{M(x_j)\sin[(x_i-x_j)/2]\pi} & for \quad i\neq j,\quad i,j=1,2,...,N_x,\\ -\sum\limits_{\substack{j=1\\ i\neq j}}^{N_x} A_{ij}^{(1)} & for \quad i=j,\quad i,j=1,2,...,N_x\end{cases} \tag{73}$$

in which

$$M(x_i)=\prod_{\substack{j=1\\ j\neq i}}^{N_x}\sin\left(\frac{(x_i-x_j)\pi}{2}\right) \tag{74}$$

Also, the higher-order derivatives are considered as

$$A_{ij}^{(n)}=n\left(A_{ii}^{(n-1)}A_{ij}^{(1)}-\pi ctg\left(\frac{x_i-x_j}{2}\right)\pi\right) \tag{75}$$

By distributing the grid points in the domain based on Eq. (72) and by substituting Eq. (71) into the governing equations, we have

$$\left(\left[\underbrace{K_L+K_{NL}}_{K}\right]\begin{Bmatrix}\{d_b\}\\ \{d_d\}\end{Bmatrix}+[M]\begin{Bmatrix}\{\ddot{d}_b\}\\ \{\ddot{d}_d\}\end{Bmatrix}\right)=\begin{Bmatrix}\{0\}\\ -Ma(t)\end{Bmatrix}, \tag{76}$$

in which $[K_L]$, $[K_{NL}]$ and $[M]$ indicate linear part of the stiffness matrix, nonlinear part of the stiffness matrix and the mass matrix, respectively. Also, $\{d_b\}$ and $\{d_d\}$ denote boundary and domain points, respectively. To obtain the time response of the structure subjected to the earthquake loads Newmark method (Simsek 2010) is applied in the time domain. Based on this method, Eq. (76) is considered in the general form as below

$$K^*(d_{i+1})=Q_{i+1}, \tag{77}$$

where subscript $i+1$ denotes the time $t=t_{i+1}$, $K^*(d_{i+1})$ and Q_{i+1} are the effective stiffness matrix and the effective load vector which are given as

$$K^*(d_{i+1})=K_L+K_{NL}(d_{i+1})+\alpha_0 M+\alpha_1 C, \tag{78}$$

$$\begin{aligned}
Q_{i+1}^*&=Q_{i+1}+M\left(\alpha_0 d_i+\alpha_2\dot{d}_i+\alpha_3\ddot{d}_i\right)\\
&+C\left(\alpha_1 d_i+\alpha_4\dot{d}_i+\alpha_5\ddot{d}_i\right),
\end{aligned} \tag{79}$$

where (Simsek 2010)

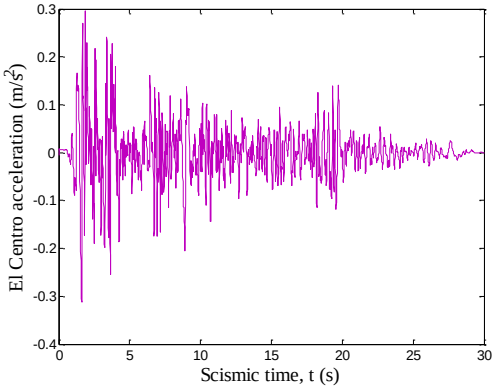

Fig. 2 Acceleration of El Centro

$$\alpha_0=\frac{1}{\chi\Delta t^2},\quad \alpha_1=\frac{\gamma}{\chi\Delta t},\quad \alpha_2=\frac{1}{\chi\Delta t},$$
$$\alpha_3=\frac{1}{2\chi}-1,\quad \alpha_4=\frac{\gamma}{\chi}-1,\alpha_5=\frac{\Delta t}{2}\left(\frac{\gamma}{\chi}-2\right), \tag{80}$$
$$\alpha_6=\Delta t\left(1-\gamma\right),\quad \alpha_7=\Delta t\gamma,$$

where γ=0.5 and χ=0.25. By applying the iteration method, Eq. (77) is solved at any time step and modified velocity and acceleration vectors are computed as follows

$$\ddot{d}_{i+1}=\alpha_0(d_{i+1}-d_i)-\alpha_2\dot{d}_i-\alpha_3\ddot{d}_i, \tag{81}$$

$$\dot{d}_{i+1}=\dot{d}_i+\alpha_6\ddot{d}_i+\alpha_7\ddot{d}_{i+1}, \tag{82}$$

Then for the next time step, the modified velocity and acceleration vectors in Eqs. (81) and (82) are applied and all the mentioned procedures are repeated.

6. Numerical results

In this section, the effect of various parameters on the dynamic response of the concrete beam reinforced by Fe_2O_3 nanoparticles under seismic load and magnetic field is examined. The length and thickness of the concrete beam are L=3 m and h=15 cm, respectively. The elastic moduli of concrete and Fe_2O_3 nanoparticles are E_c=20 GPa and E_r=209 GPa, respectively. The earthquake acceleration is considered based on El Centro earthquake that the distribution of acceleration in 30 seconds is shown in Fig. 2.

6.1 Convergence of HDQM

Fig. 3(a)-(d) shows the convergence of HDQM in evaluating the maximum deflection of the structure versus time. As it can be seen, with increasing the number of grid points N, the maximum deflection of the structure decreases until N=15, which the results converge to a constant value. So, the results presented below are based on the number of grid points 15 for HDQ solution method.

6.2 Validation of results

Since, there is not any similar work in the literature in the scope of this paper, however, validation of this work is done by comparing the numerical and analytical solutions. The results of the analytical and numerical (HDQ) methods are depicted in Fig. 4. As it can be observed, the results of numerical and analytical methods are identical and therefore, the obtained results are accurate and acceptable.

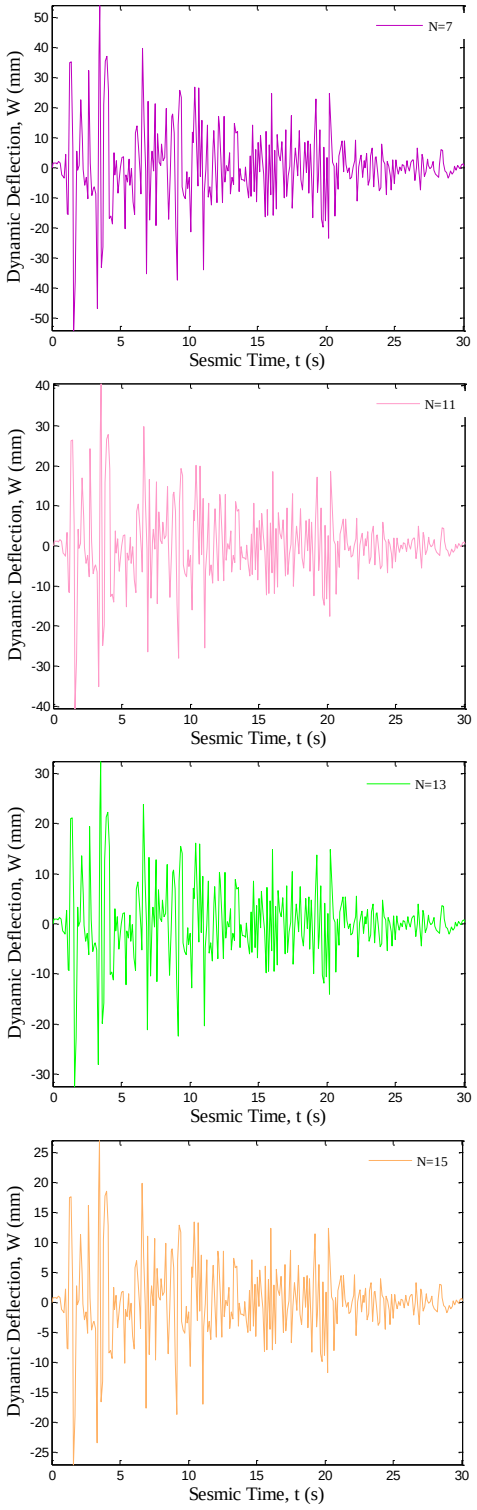

Fig. 3 Convergence and accuracy of HDQM

6.3 Effect of magnetic field

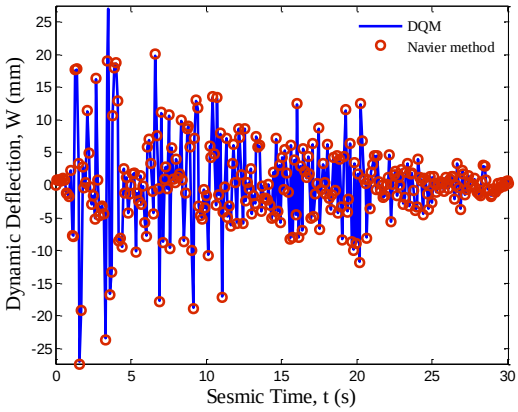

Fig. 4 Comparison of numerical and analytical results

Fig. 5 (a)-(d) illustrate the effect of magnetic field on the dynamic deflection versus time. As it can be observed, the structure without magnetic field has a greater dynamic deflection with respect to the concrete beam subjected to magnetic field. The reason is that the magnetic field increases the stiffness of the structure. Fig. 5(a) shows the maximum dynamic deflection of the structure without magnetic field equal to 39 while by applying the magnetic field of 1, 5 and 10 A/m, the maximum dynamic displacement of the structure is 27.05, 18.15 and 17.97, respectively. By comparing the results, we can say that applying the magnetic field of 1, 5 and 10 A/m decreases the maximum dynamic displacement of the structure up to 30.64, 53.46 and 53.92 percent which is a remarkable result in the dynamic designing of the structures. Also it should be noted that the excessive increasing of the magnetic field increases costs while it does not have a noticeable effect on the dynamic response of the structure. Hence, the magnetic field of 5 A/m is the best choice for the present structure.

6.4 Effect of Fe_2O_3 nanoparticles

The effect of Fe_2O_3 nanoparticles volume percent on the dynamic response of the structure is studied. Fig. 6(a)-(d). It is apparent that the maximum dynamic displacement of the structure is equals to 32.3 for the case of c_r=0 (without Fe_2O_3 nanoparticles). By using Fe_2O_3 nanoparticles with volume fractions of 0.05, 0.1 and 0.18, the amount of maximum dynamic displacement is 29.1, 27.05 and 30.83, respectively. Therefore, using Fe_2O_3 nanoparticles with volume fractions of 0.05 and 0.1 increases the stiffness of the structure and reduces the maximum displacement of structure 9.91 and 16.25 percent, respectively while the volume percent of 0.18 has a converse result and 4.5 percent increase the deflection.

The agglomeration effect of Fe_2O_3 nanoparticles on the dynamic deflection of the structure versus time is illustrated in Fig. 7(a)-(d). As it can be observed, by considering the agglomeration effect, the stiffness of the structure reduces while the dynamic displacement increases. For example, in the absence of the agglomeration effect (ξ=1), the maximum dynamic deflection of the structure is 22.22 while for ξ=0.5 the maximum dynamic deflection is 27.05. The results reveal that the existence of the agglomeration changes the maximum dynamic displacement of the structure up to 21.74 percent.

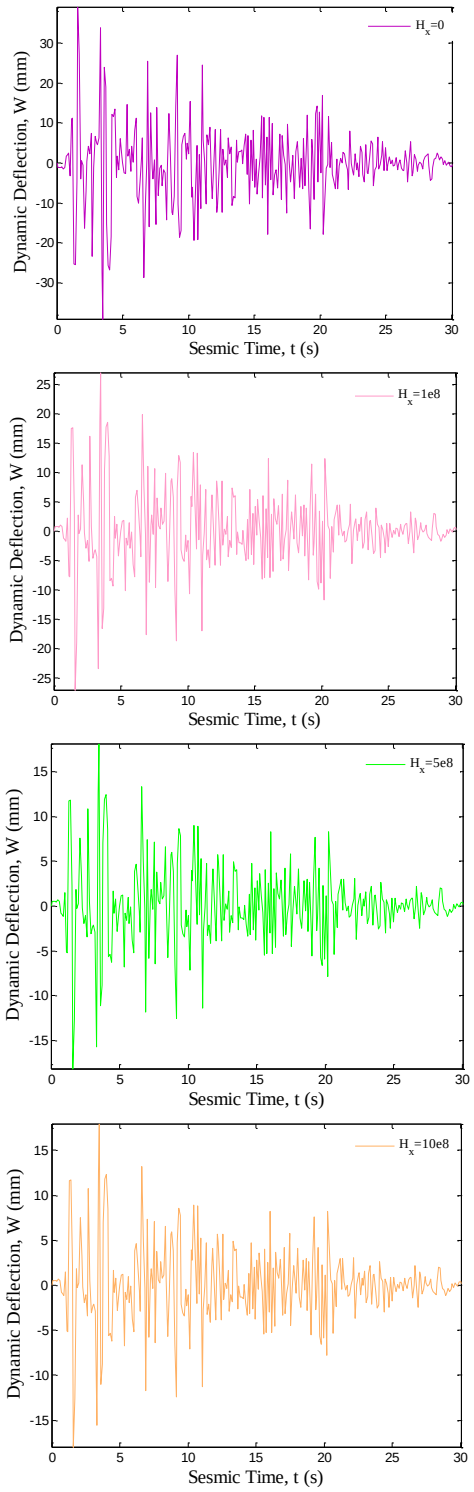

Fig. 5 The effect of magnetic field on the dynamic response of the structure

6.5 Effect of concrete beam length

The effect of concrete beam length on the dynamic response versus time is shown in Fig. 8(a)-(d). It can be seen that with an increase in the concrete beam length, the

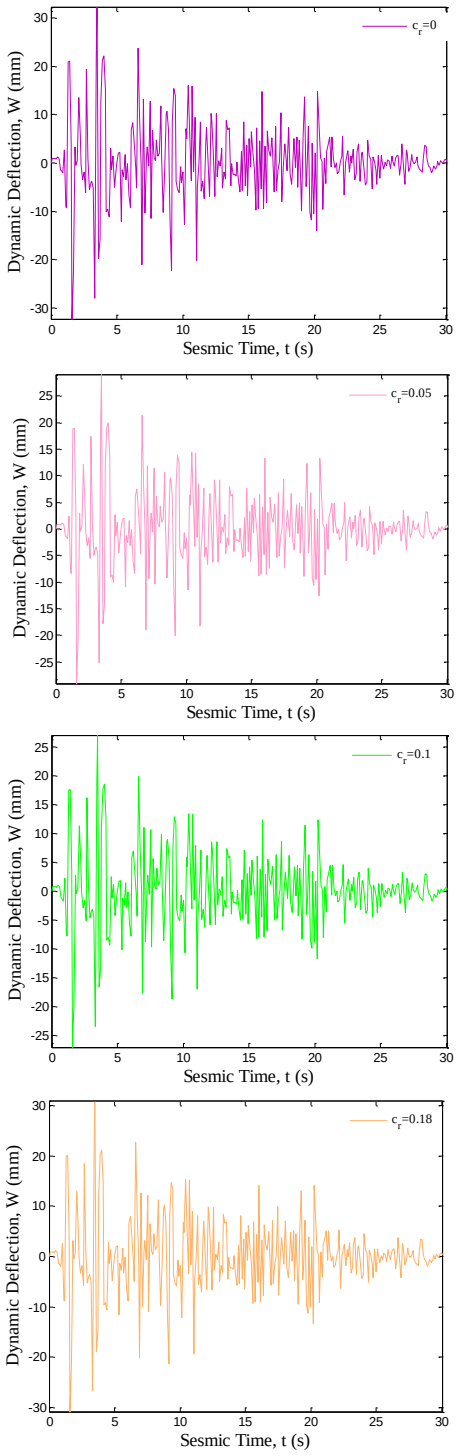

Fig. 6 The effect of Fe_2O_3 nanoparticles volume percent on the dynamic response of the structure

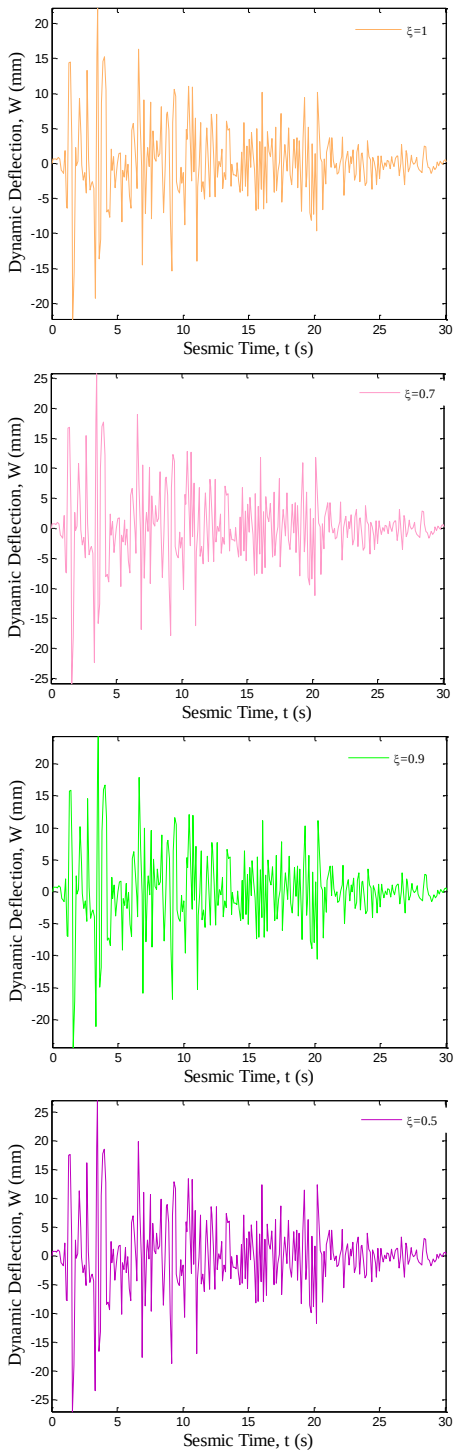

Fig. 7 The effect of Fe_2O_3 nanoparticles agglomeration on the dynamic response of the structure

structure becomes softer and the dynamic deflection of the system increases. For example, the maximum dynamic displacements of the concrete beam increase 72.75% with increasing the length from 2 to 3 m.

6.6 Effect of boundary conditions on dynamic response

Fig. 9(a)-(d) illustrate the effect of various boundary conditions on the dynamic response versus time. Four boundary conditions including clamped-clamped, clamped-simply, simply-simply and free-simply supported are considered. The maximum dynamic deflections of the structure for clamped-clamped, clamped-simply supported, simply-simply supported and free-simply supported boundary conditions are 13.53, 18.94, 27.05 and 32.46, respectively. As it can be observed, boundary conditions have a significant effect on the dynamic response of the

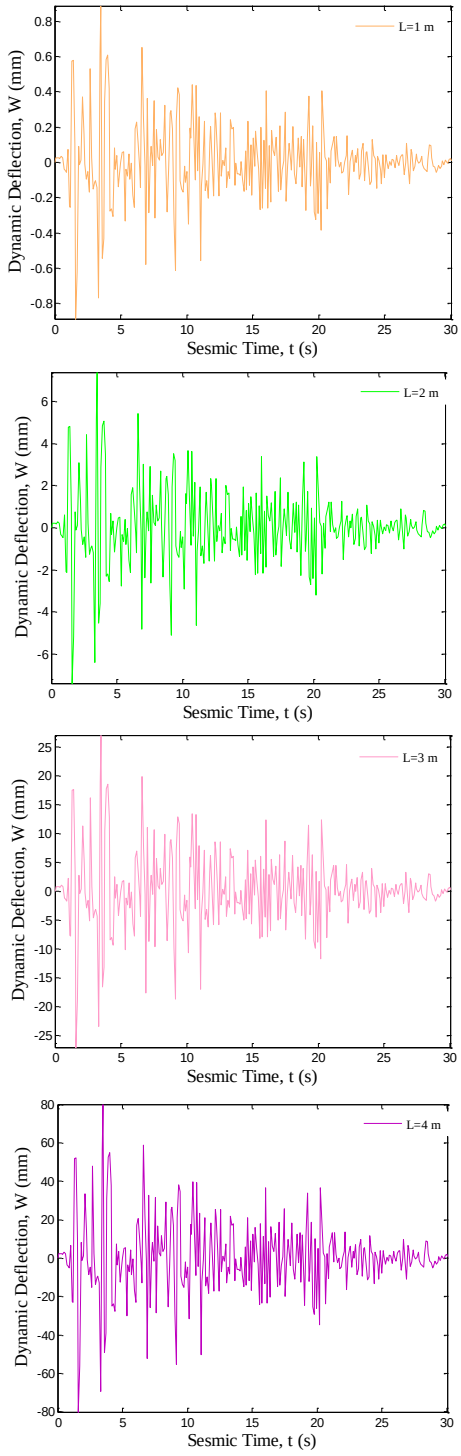

Fig. 8 The effect of concrete beam length on the dynamic response of the structure

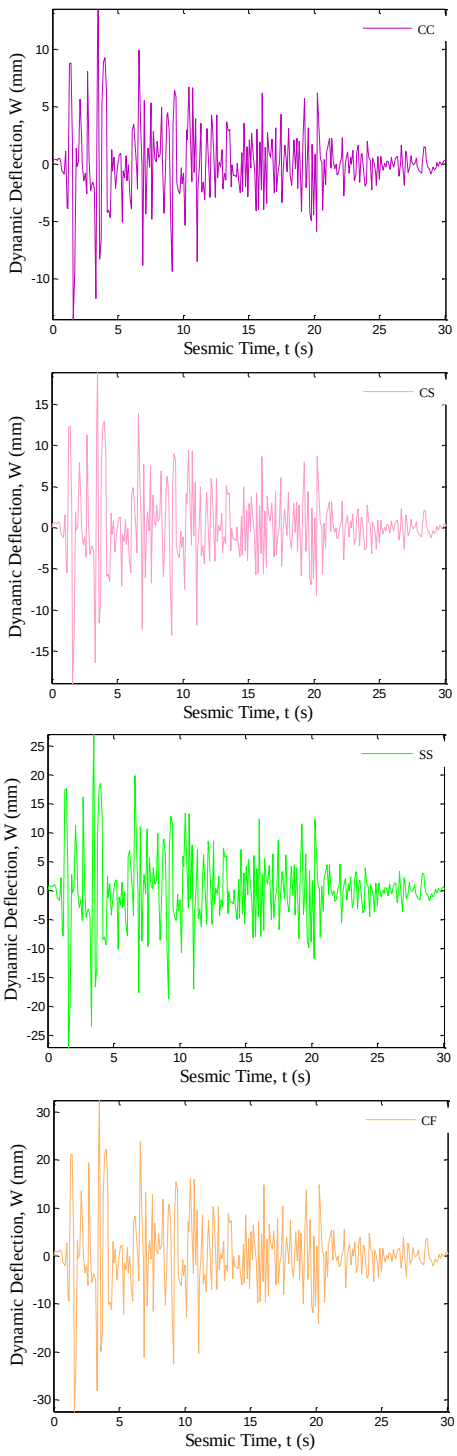

Fig. 9 The effect of different boundary conditions on the dynamic response of the structure

system so that the structure with clamped-clamped boundary condition has the lowest displacement with respect to the other boundary conditions.

7. Conclusions

Seismic response of concrete beams reinforced by Fe_2O_3 nanoparticles was presented in this article. The structure was subjected to axial magnetic field for controlling the dynamic deflection of the structure. Based on HSDBT, the structure was simulated and utilizing the energy method and Hamilton's principle, the motion equations were derived. For calculating the effective material properties of structure and considering agglomeration of Fe_2O_3 nanoparticles, Mori-Tanaka model was used. Applying HDQ and Newmark methods, the dynamic deflection of the structure was calculated and the effects of different parameters of

Fe_2O_3 nanoparticles volume percent and agglomeration, magnetic field, boundary conditions and length of the concrete beam were considered on the results. Numerical results indicate that the structure without magnetic field has a greater dynamic deflection with respect to the concrete beam subjected to magnetic field so that applying the magnetic field of 5 A/m decreases the maximum dynamic displacement of the structure up to 53.46 percent. Also it should be noted that the excessive increasing of the magnetic field increases costs while it does not have a noticeable effect on the dynamic response of the structure. Using Fe_2O_3 nanoparticles with volume fractions of 0.05 and 0.1 increases the stiffness of the structure and reduces the maximum displacement of structure 9.91 and 16.25 percent, respectively while the volume percent of 0.18 has a converse result and 4.5 percent increase the deflection. The results reveal that the existence of the agglomeration changes the maximum dynamic displacement of the structure up to 21.74 percent. In addition, the maximum dynamic displacements of the concrete beam increase 72.75% with increasing the length from 2 to 3 m. Furthermore, boundary conditions have a significant effect on the dynamic response of the system so that the structure with clamped-clamped boundary condition has the lowest displacement with respect to the other boundary conditions.

References

Alibeigloo, A. (2016), "Thermoelastic analysis of functionally graded carbon nanotube reinforced composite cylindrical panel embedded in piezoelectric sensor and actuator layers", *Compos. Part B: Eng*., **98**, 225-243.

Cao, V.V. and Ronagh, H.R. (2014), "Reducing the potential seismic damage of reinforced concrete frames using plastic hinge relocation by FRP", *Compos. Part B: Eng.*, **60**, 688-696.

Changwang, Y., Jinqing, J. and Ju, Z. (2010), "Seismic behavior of steel reinforced ultra high strength concrete column and reinforced concrete beam connection", *Trans. Tianjin Univ.*, **16**, 309-316.

Cheng, C. and Chen, C. (2004), Seismic behavior of steel beam and reinforced concrete column connections", *J. Constr. Steel Res*., **61**, 587-606.

Choi, S.W., Yousok, K. and Park, H.S. (2014), "Multi-objective seismic retrofit method for using FRP jackets in shear-critical reinforced concrete frames", *Compos. Part B: Eng*., **56**, 207-216.

Davar, A., Khalili, S.M.R. and Malekzadeh Fard, K. (2013), "Dynamic response of functionally graded circular cylindrical shells subjected to radial impulse load", *Int. J. Mech. Mater. Des*., **9**, 65-81.

Feng, Ch., Kitipornchai, S. and Yang, J. (2017), "Nonlinear bending of polymer nanocomposite beams reinforced with non-uniformly distributed graphene platelets (GPLs)", *Compos. Part B: Eng*., **110**, 132-140.

Formica, G., Lacarbonara, W. and Alessi, R. (2010), "Vibrations of carbon nanotube reinforced composites", *J. Sound Vib*., **329**, 1875-1889.

GhorbanpourArani, A., Haghparast, E., KhoddamiMaraghi, Z. and Amir, S. (2015), "Static stress analysis of carbon nano-tube reinforced composite (CNTRC) cylinder under non-axisymmetric thermo-mechanical loads and uniform electro-magnetic fields", *Compos. Part B: Eng*., **68**, 136-145.

JafarianArani, A. and Kolahchi, R. (2016), "Buckling analysis of embedded concrete columns armed with carbon nanotubes", *Comput. Concrete*, **17**, 567-578.

Ji, X., Zhang, M., Kang, H., Qian, J. and Hu, H. (2014), "Effect of cumulative seismic damage to steel tube-reinforced concrete composite columns", *Eartq. Struct*., **7**, 179-200.

Kolahchi, R., RabaniBidgoli, M., Beygipoor, Gh. and Fakhar, M.H. (2013), "A nonlocal nonlinear analysis for buckling in embedded FG-SWCNT-reinforced microplates subjected to magnetic field", *J. Mech. Sci. Tech*., **5**, 2342-2355.

Kolahchi, R., Safari, M. and Esmailpour, M. (2016), "Dynamic stability analysis of temperature-dependent functionally graded CNT-reinforced visco-plates resting on orthotropic elastomeric medium", *Compos. Struct.*, **150**, 255-265.

Lei, Z.X., Zhang, L.W., Liew, K.M. and Yu, J.L. (2014), "Dynamic stability analysis of carbon nanotube-reinforced functionally graded cylindrical panels using the element-free kp-Ritz method", *Compos. Struct.*, **113**, 328-338.

Liang, X. and Parra-Montesinos, G.J. (2004), "Seismic behavior of reinforced concrete column-steel beam subassemblies and frame systems", *J. Struct. Eng.*, **130**, 310:319.

Liew, K.M., Lei, Z.X., Yu, J.L. and Zhang, L.W. (2014), "Postbuckling of carbon nanotube-reinforced functionally graded cylindrical panels under axial compression using a meshless approach", *Comput. Meth. Appl. Mech. Eng*., **268**, 1-17.

Liu, Z.Q., Xue, J.Y. and Zhao, H.T. (2016), "Seismic behavior of steel reinforced concrete special-shaped column-beam joints", *Eartq. Struct.*, **11**, 665-680.

Matsuna, H. (2007), "Vibration and buckling of cross-ply laminated composite circular cylindrical shells according to a global higher-order theory", *Int. J. Mech. Sci.*, **49**, 1060-1075.

Mori, T. and Tanaka, K. (1973), "Average stress in matrix and average elastic energy of materials with misfitting inclusions", *Acta Metall. Mater*., **21**, 571-574.

Shen, H.S. and Yang, D.Q. (2014), "Nonlinear vibration of anisotropic laminated cylindrical shells with piezoelectric fiber reinforced composite actuators", *Ocean Eng*., **80**, 36-49.

Shu, C. and Xue, H. (1997), "Explicit computations ofweighting coefficients in the harmonic differential quadrature", *J. Sound Vib*., **204**(3), 549-555.

Simsek, M. (2010), "Non-linear vibration analysis of a functionally graded Timoshenko beam under action of a moving harmonic load", *Compos. Struct.*, **92**, 2532-2546.

Simsek, M. and Reddy, J.N. (2013), "A unified higher order beam theory for buckling of a functionally graded microbeam embedded in elastic medium using modified couple stress theory", *Compos. Struct.*, **101**, 47-58.

Wuite, J. and Adali, S. (2005), "Deflection and stress behaviour of nanocomposite reinforced beams using a multiscale analysis", *Compos. Struct.*, **71**, 388-396.

Zamani, A., Kolahchi, R. and Rabani Bidgoli, M. (2017), "Seismic response of smart nanocomposite cylindrical shell conveying fluid flow using HDQ-Newmark methods", *Comput. Concrete*, **20**, 671-682.

Zarei, M.Sh., Kolahchi, R., Hajmohammad, M.H. and Maleki, M. (2017), "Seismic response of underwaterfluid-conveying concrete pipes reinforced with SiO_2 nanoparticles andfiber reinforced polymer (FRP) layer", *Soil Dyn. Earthq. Eng.*, **103**, 76-85.

CC